Voltage-Impulse-Induced Nonvolatile Control of Inductance in Tunable Magnetoelectric Inductors

Bin Peng, Chenxi Zhang, Yuan Yan, and Ming Liu*

Electronic Materials Research Laboratory, Key Laboratory of the Ministry of Education & International Center for Dielectric Research, Xi'an Jiaotong University, Xi'an 710049, China

(Received 26 December 2016; revised manuscript received 9 March 2017; published 19 April 2017)

In this work, nonvolatile magnetoelectric tunable inductors are developed based on Metglas/(011) $Pb(Mg_{1/3}Nb_{2/3})O_3$-$PbTiO_3$ multiferroic composites. They exhibit a large nonvolatile tunability up to 250% at 10 kHz and 120% at 1 MHz, in which the voltage control of inductance is achieved through strain-mediated magnetoelastic anisotropy. Such high nonvolatile tunability is attributed to a dramatic change of the in-plane lattice strain arising from non-180° ferroelastic domain switching in $Pb(Mg_{1/3}Nb_{2/3})O_3$-$PbTiO_3$. Electric field dependent inductance is then calculated from the strain-induced effective magnetic field and effective permeability change, and it is consistent with our experimental results. Engineering of ferroelastic domain states in multiferroic composites provides a pathway to realize nonvolatile electrically tunable inductors for lightweight, compact, power-efficient integrated power electronics, rf devices, and systems.

DOI: 10.1103/PhysRevApplied.7.044015

I. INTRODUCTION

Inductors, as one of the three fundamental passive components, have been extensively used in communication systems and power electronics, such as voltage regulation, oscillators, filters, and matching networks [1,2]. Recently, tunable inductors have become highly desirable due to the ability to optimize the performance of electrical circuits in situ and miniaturize electronic devices [3–14]. Great efforts have been devoted to electrically tunable inductors that have large tunability, high quality factor (Q), and low energy consumption. Traditional tunable inductors were controlled mechanically or by current-driven electromagnets, which are bulky, noisy, and energy consuming [12–14]. Though the microelectromechanical systems (MEMS) approach [7,10,15–18] is promising for tunable inductors used in highly integrated systems, the relatively large driving current (tens of milliamperes) introduces additional power consumption.

Recently, multiferroic-composite-based magnetoelectric (ME) tunable inductors exhibiting giant tunability and voltage control of inductance (L) have been showing a great advantage for application in power-efficient integrated systems [3–6,19]. In these devices, multiferroic composites consisting of ferromagnetic materials and ferroelectric materials are employed. Strain arising from ferroelectric materials can be transferred to ferromagnetic materials through the interfacial mechanical coupling so that the magnetic properties are modulated and result in the change of magnetic anisotropy [20]. Fang *et al.* [19] reported that the permeability of MnZn ferrite could be tuned by 20%, which was observed from a ring-type inductor with a bar of lead zirconate titanate (PZT) mounting in the center. Later, Liu *et al.* [4] fabricated a MnZn-ferrite/PZT–laminate-based ring-type ME inductor, and its tunability improved to 56% through interface-strain coupling. Lou *et al.* [6] reported a solenoid-type ME inductor with giant tunability up to 450% as well as an improved quality factor. Because of eddy current loss, its operating frequency range was limited to < 100–200 kHz. Later, they reported by reducing the thickness of magnetic ribbons, the operating frequency range can be extended up to 100 MHz with significantly enhanced quality factor (approximately 15.3) [5]. In those reports, ME tunable inductors had to be operated under a constant voltage as a linear piezoelectric strain effect was employed, which could release the device to the initial state after removing the voltage. Electrostatically nonvolatile control of inductance is much more desirable for reducing power but still remains challenging. It was reported recently that the asymmetric strain electric field response could be used for nonvolatile control of inductance in ME inductors through defect engineering in ferroelectric materials [3]. However, this special requirement may cause ferroelectric fatigue [21], which will influence the reliability of ME inductors.

In this paper, voltage-impulse-induced nonvolatile control of inductance is demonstrated in ME tunable inductors based on Metglas/(011) $Pb(Mg_{1/3}Nb_{2/3})O_3$-$PbTiO_3$ (PMN-PT) multiferroic composites. Giant nonvolatile inductance tunability up to 250% is achieved. The underlying mechanism is upon lattice-strain-induced magnetic anisotropy change, and this dramatic lattice strain is from

*To whom all correspondence should be addressed.
mingliu@xjtu.edu.cn

non-180° ferroelastic domain switching of PMN-PT. A nearly linear control of inductance by voltage impulses is achieved, showing its great advantage for potential applications in compact and power-efficient integrated circuits and systems.

II. EXPERIMENT

Commercially available Metglas 2605SA1 ribbons (Metglas, Inc.), an iron-based amorphous alloy, are used as the magnetic core of the inductors, and their thickness is about 25 ± 4 μm. (011)-cut PMN-PT single-crystal slabs are used as piezoelectric layers, which have a dimension of 5 mm (width) $\times$ 10 mm (length) $\times$ 0.5 mm (thickness) in which the [100] direction is parallel to the length direction, and the $[01\bar{1}]$ direction is parallel to the width direction. The rhombohedral PMN-PT slabs are polished, and both sides are coated with silver electrodes for electrical connection. They are saturationally poled by the manufacturer. Metglas ribbons ($5 \times 8\text{mm}^2$) are tightly bonded to both sides of the PMN-PT slabs by epoxy glue, and 40–60 turns of the copper coil are wound onto the multiferroic composites. A dc voltage ranging from -600 to 600 V is applied across the thickness direction of the piezoelectric slabs by a voltage source (Keithley 6517B), and the inductance and quality factor are measured by a precision *LCR* meter (Agilent E4980A).

III. RESULTS AND DISCUSSION

A. Electric field and frequency dependence of inductance

Figure 1(a) shows the schematic of solenoid-type ME tunable inductors with Metglas/PMN-PT/Metglas multiferroic composites as a magnetic core and a prototype of ME tunable inductors. The magnetic flux direction is parallel to the [100] direction of the (011) PMN-PT. Figure 1(b) shows the electric field dependence of inductance over a wide frequency range from 1 kHz to 2 MHz, and Fig. 1(c) shows the corresponding quality factor. In the initial state, the inductance L starts at about 8.8 μH at 1 kHz, and it slightly decreases with increasing frequency, accompanied by an enhanced quality factor >10 of which the maximum occurs at about 800 kHz. The reduction of inductance at high frequency is related to the large eddy current screening effect [5,6], which diminishes the effective permeability at high frequency dramatically. Upon applying a positive electric field of 12 kV/cm, the inductance increases due to the piezoelectric effect, which is determined to be 13 μH at 1 kHz. Since the eddy current at high frequencies introduces a strong magnetic loss, the critical frequency limit is also dependent on the effective permeability when the magnetic layer thickness is larger than its skin depth [6]. Consequently, the quality-factor peak shifts downward with the enhanced permeability or

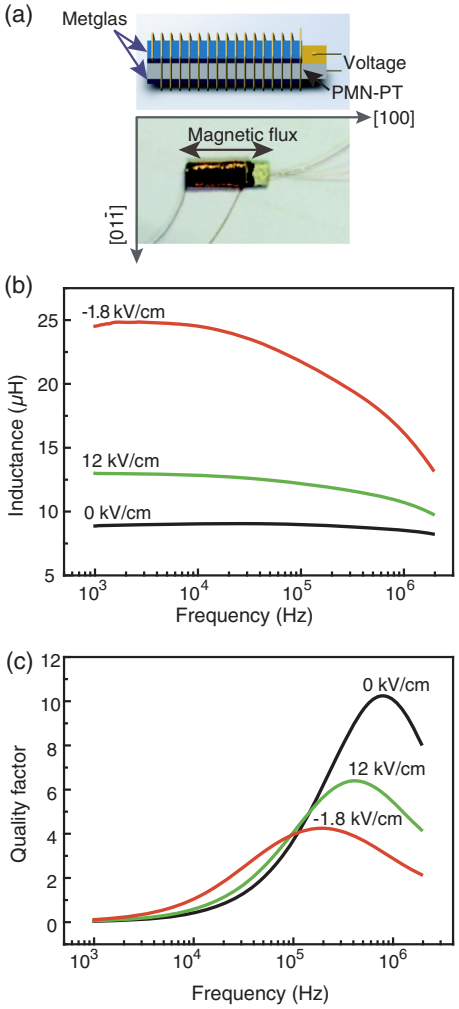

FIG. 1. (a) Schematic of ME tunable inductors (top) based on Metglas/(011) PMN-PT multiferroic composites and a prototype of the ME inductor (bottom). The [100] direction of the PMN-PT is along the length direction, and the $[01\bar{1}]$ direction is along the width direction. (b) Inductance-frequency response under different electric fields (0, 12, and -1.8 kV/cm) and the corresponding (c) quality-factor frequency response.

inductance. In addition, the linear piezoelectric effect results in a 48% change of inductance at 1 KHz.

However, as a small negative electric field of -1.8 kV/cm is applied, which is close to the coercive field of (011) PMN-PT, the inductance increases significantly, and tunability can be over 250% at 1 kHz. Compared to the linear piezoelectric effect, this negative electric field induced larger inductance as well as larger tunability, indicating the [100] direction becomes much easier with the greater magnetization component along the [100] direction.

Figure 2(a) shows the inductance in response to *in situ* bipolar electric fields. A "butterfly" curve is observed as cycling triangle electric fields within ± 12 kV/cm, showing a maximum tunable inductance range from 8.0 to 28.1 μH. Upon applying a negative electric field on a positively

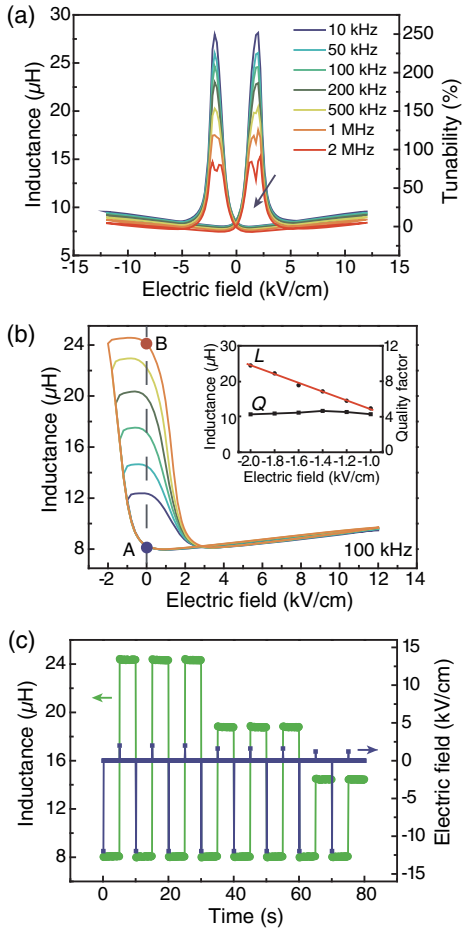

FIG. 2. Voltage control of inductance in Metglas/(011) PMN-PT multiferroic-composite-based ME tunable inductors. (a) Inductance as a function of bipolar electric field of ±12 kV/cm at different frequencies (10 kHz to 2 MHz). (b) Inductance as a function of quasiunipolar electric field at 100 kHz. The inset shows the inductance and quality factor when removing the negative electric field to zero. (c) Voltage-impulse-induced nonvolatile switching of inductance at 100 kHz.

poled ME tunable inductor, a giant inductance jump takes place near the coercive field of −2 kV/cm. Figure 2(b) shows the inductance change under the quasiunipolar electric field from 12 to −2 kV/cm at the measuring frequency of 100 kHz. When removing the positive electric field, a remnant low-inductance state "*A*" is obtained. However, by the removal of that negative electric field close to the coercive field, the enhanced inductance can be maintained, and a new remnant high-inductance state "*B*" is obtained. Moreover, this remnant high-inductance state has a nearly linear relationship with the amplitude of negative electric field, which is shown in the inset of Fig. 2(b). The distinct low- and high-inductance states after removal of the electric field facilitate the realization of nonvolatile control of inductance by reversing the applied electric field near the coercive field. Additionally, the quality factor remains relatively high and stable during nonvolatile control.

Figure 2(c) shows the voltage-impulse-induced nonvolatile switching of inductance in Metglas/(011) PMN-PT ME tunable inductors. As the (011) PMN-PT is subjected to an impulse of −12 kV/cm, a minimum inductance of 8.2 μH at 100 kHz is obtained. Upon applying an impulse field of 2 kV/cm, the inductance increases to the maximum of 24.4 μH. Furthermore, reversing the bias to an impulse of −12 kV/cm can reset the inductance to its minimum value again. In addition to nonvolatile switching between the minimum and the maximum, any inductance between them is reachable by choosing a proper positive voltage-impulse. For example, the inductance of 14.4 μH can be realized by applying pulsed electric fields of −12 and 1.2 kV/cm. Applying different levels of positive voltage-impulse can set the inductance to different levels, and they remain stable during repeated measurement.

Voltage control of the magnetism in multiferroic-composite-based ME tunable inductors is due to interfacial strain coupling [22]. Electric field induces strain in the ferroelectric layer due to either the piezoelectric effect or ferroelectric domain switching. It is then transferred to the ferromagnetic layer and alters its magnetoelastic anisotropy. This strain-mediated magnetoelastic anisotropy change in the ferromagnetic layer can be interpreted as an effective magnetic field (H_{ME}) [20]

$$H_{\mathrm{ME}} = \frac{3\lambda_s(\sigma_{100} - \sigma_{01\bar{1}})}{M_s}, \tag{1}$$

where σ_{100} and $\sigma_{01\bar{1}}$ are the in-plane stress along the [100] and $[01\bar{1}]$ directions, and M_s is the saturation magnetization. Because Metglas ribbons have an intrinsic anisotropy field H_a, the total effective magnetic field $H_{\mathrm{eff}} = H_a + H_{\mathrm{ME}}$ along the magnetic flux direction ([100] direction) highly depends on the biaxial in-plane strain or stress in (011) PMN-PT. Since the Metglas ribbons have a positive magnetostriction $\lambda_s = 27$ ppm, compressive strain or stress is expected to favor magnetic easy axis, while tensile strain or stress is opposite. As the (011) PMN-PT is positively poled, applying a positive electric field will create a negative H_{ME} in ME tunable inductors because of tensile strain or stress along the $[01\bar{1}]$ direction and compressive strain or stress along the [100] direction [23]. As the effective permeability μ_{eff} is inversely proportional to H_{eff} [6,14],

$$\mu_{\mathrm{eff}} = 4\pi M_s/H_{\mathrm{eff}} + 1, \tag{2}$$

the linear piezoelectric effect makes the inductance increase, as observed in Fig. 2.

B. Ferroelastic domain-switching-induced nonvolatile behavior

The nonvolatile tuning of inductance in Metglas/(011) PMN-PT ME tunable inductors can be attributed to the stable and reversible ferroelastic domain switching in

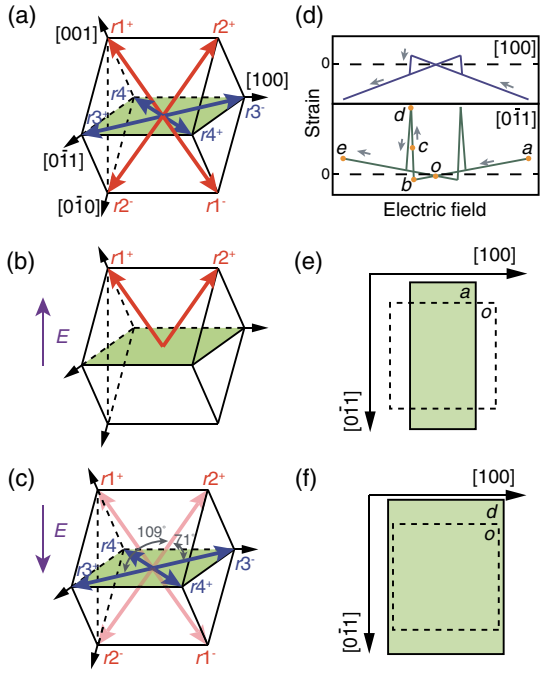

FIG. 3. Schematic illustration of ferroelastic domain switching and in-plane strain change of (011) PMN-PT: polarization orientations within a pseudocubic unit cell at (a) random, (b) fully poled, (c) partially depolarized states for (011) rhombohedral PMN-PT, (d) schematic illustration of in-plane strain-electric field response and in-plane deformation at (e) fully poled and (f) partially depolarized states.

(011) PMN-PT [24,25]. Figure 3 schematically illustrates ferroelectric domain switching and the corresponding in-plane deformation of (011) PMN-PT. In rhombohedral PMN-PT single crystals, polarization can align along eight-body diagonal directions of the pseudocubic unit cell with four structural domains ($r1$, $r2$, $r3$, $r4$) [26] as shown in Fig. 3(a). With the application of a large positive electric field, PMN-PT will be saturationally poled with polarization pointing to $r1^+/r2^+$ [Fig. 3(b)], and it can remain in $r1^+/r2^+$ after removing the electric field to zero. Then, applying a small negative electric field PMN-PT will be partially depolarized, and some polarization will switch through the pathways including the 71° domain switching from $r1^+$ to $r3^+/r4^-$ or $r2^+$ to $r3^-/r4^+$, 109° domain switching from $r1^+$ to $r4^+/r3^-$ or $r2^+$ to $r3^+/r4^-$, and 180° domain switching from $r1^+$ to $r1^-$ or $r2^+$ to $r2^-$ as indicated in Fig. 3(c). Both 71° and 109° ferroelectric or ferroelastic domain switching are accompanied by the change of in-plane lattice strain, while 180° domain switching induces zero net strain. Since the energy barrier for non-180° (71° and 109°) domain switching is smaller than that of 180° domain switching, non-180° domain switching is favored under small negative electric fields. With this negative field further reducing, more and more domains undergo non-180° ferroelastic domain switching. Figure 3(c) shows that in an extreme situation, (011) PMN-PT is fully depolarized with most of the out-of-plane polarizations rotating to in-plane directions.

Figure 3(d) schematically illustrates in-plane strain electric field response based on *in situ* lattice change [24] and directly measured curves of (011) PMN-PT [23,27]. Path *a-o-b* indicates a linear piezoelectric-effect-induced strain along the $[01\bar{1}]$ direction, and a positive piezoelectric coefficient introduces positive strain when applying the positive electric field and negative strain when applying the small negative electric field. The reverse behavior can be observed along the [100] direction. Path *b-c-d* indicates ferroelectric domain-switching-induced strain, and with more and more polarization switching to in plane, the lateral dimension of PMN-PT will expand to introduce positive strain along both [100] and $[01\bar{1}]$ directions. Figures 3(e) and 3(f) show in-plane deformation corresponding to fully polarized and depolarized states, respectively, with the application of electric field, and the dashed rectangle indicates a saturationally poled state at zero electric field. The linear piezoelectric effect induces volatile compressive strain (−0.05% [23]) along the [100] direction and tensile strain along the $[01\bar{1}]$ direction (0.02% [23]), and non-180° ferroelastic domain switching induces large tensile strain (0.13% [23] or 0.25% [24], depending on electric field) along the $[01\bar{1}]$ direction with small lattice-strain variation along the [100] direction (0.02% [23]). Consequently, the inductance will be enhanced in both the linear region *a-o* and the nonvolatile region *b-c-d* because of reduced H_{ME} and H_{eff}. Moreover, the in-plane $r3^+/r3^-$ and $r4^+/r4^-$ orientations are stable polarization orientations, and these domains will remain stable after removing the electric field, so the depolarization state and the corresponding in-plane deformation are stable. Hence, nonvolatile control of inductance can be achieved through voltage-impulse stimulus to ME tunable inductors.

Given a directly measured in-plane [100] and $[01\bar{1}]$ strain electric field response [23,27], voltage control of inductance can be calculated. First, the electric field control of H_{ME} along the [100] direction of (011) PMN-PT is calculated, and in-plane stress is transformed from strain by Hooke's law [20],

$$H_{\mathrm{ME}} = \frac{3\lambda_s Y(\varepsilon_{100} - \varepsilon_{01\bar{1}})}{M_s(1+\nu)}, \tag{3}$$

where Y is Young's modulus, which is 110 GPa and $M_s = 1.56$ T, [28] υ is Poisson's ratio of 0.32, and ε_{100} and $\varepsilon_{01\bar{1}}$ are the in-plane principal strains. Figure 4(a) shows the calculated H_{eff} under quasiunipolar electric field. It changes linearly from 42 to 80 Oe with electric field decrease from 6 to 0 kV/cm. Further reducing the electric field, H_{eff} first slightly changes, then decreases dramatically to 10 Oe near −1 kV/cm, and remains relatively stable after returning to 0 kV/cm. A dramatic enhancement of H_{eff} is observed again with positive electric field

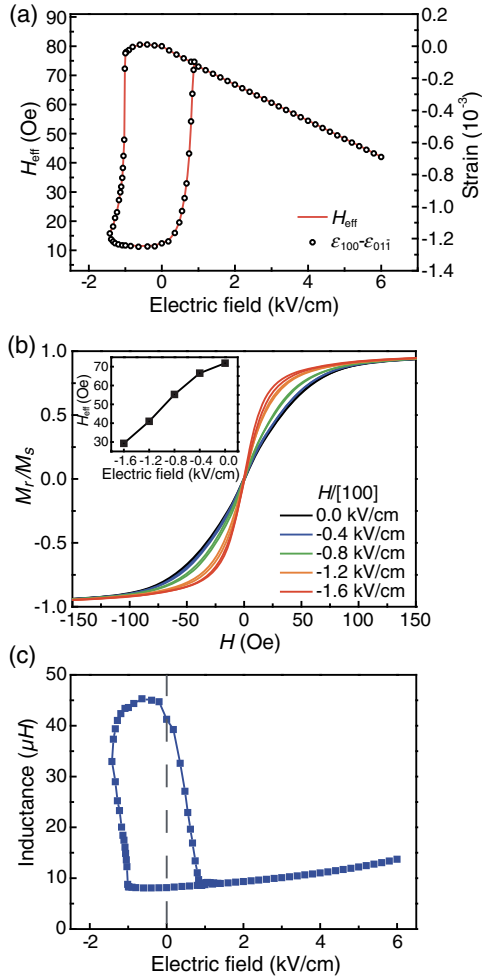

FIG. 4. (a) Unipolar electric field dependence of the in-plane strain difference $\varepsilon_{100} - \varepsilon_{01\bar{1}}$ [reproduced from T. Wu, A. Bur, P. Zhao, K. P. Mohanchandra, K. Wong, K. L. Wang, C. S. Lynch, and G. P. Carman, Appl. Phys. Lett. 98, 012504 (2011). Copyright 2011, AIP Publishing] and the calculated induced effective anisotropy field H_{eff}. (b) M-H loops measured under different electric fields along the [100] direction of the (011) PMN-PT. (c) The calculated unipolar inductance electric field curve.

increasing, and it coincides with the first branch at high electric fields. Figure 4(a) demonstrates both linear and nonvolatile control of H_{eff}, and the latter is very obvious. Figure 4(b) shows M-H hysteresis loops of the multiferroic composites under different electric fields measured along the [100] direction. The total effective anisotropy field can be directly estimated. Apparently, applying a positive electric field and then returning to zero results in a large effective magnetic field of about 71 Oe. Then, by applying the negative electric field impulse, it reduces to about 30 Oe. This directly measured effective magnetic field is very close to the calculated ones, and the difference between them may lie in the composition variation of PMN-PT between the reported one [23,27] and the one used here with different coercive field and effectiveness of strain transferring between the Metglas ribbons and PMN-PT as they are bonded by epoxy glue. Based on the above analysis, the inductance is then simulated as follows [6]:

$$L = \mu_0 \frac{2\mu_{\text{eff}} t + (d - 2t)}{d} \frac{N^2 A}{l}, \tag{4}$$

where N is the number of turns of the coil, A is the cross-section area of the coil, l is the length of the coil, t is the total thickness of the Metglas ribbons, and d is the height of the core. Figure 4(c) shows the calculated quasiunipolar L-E curve which shows similar behavior as the experimental observation in Fig. 2(b). The discrepancy is likely due to the effectiveness of strain transferring as the Metglas ribbons are bonded to piezoelectric single-crystal slabs by epoxy glue. The large difference in mechanical properties between organic epoxy glue and piezoelectric single crystals influences the transferring efficiency, which has a strong impact on the magnetoelectric coupling strength [29].

Though the asymmetric electric-field-strain response of ferroelectric materials achieved by defect engineering can also be employed for nonvolatile control of inductance [3], the tunability is limited to less than 40% due to the inherent restricted piezoelectric response. It may also induce ferroelectric fatigue [21], which may weaken the reliability of ME tunable inductors. In contrast, large residual strain induced by non-180° ferroelastic domain switching is always observed in ferroelectric materials [24,30,31], regardless of defect engineering. Hence, this feature guarantees not only a giant tunability up to 250% studied here, but it also provides many more choices of ferroelectric or piezoelectric materials, e.g., environmentally friendly lead-free piezoelectrics-based [32] ME tunable inductors. Finally, it is easy to adjust the inductance of the ME tunable inductors to different levels by simple variation of the voltage impulse. By reducing the eddy current in magnetic ribbons [5], nonvolatile ME tunable inductors with both giant tunability and high Q will be readily available for lightweight, compact, and power-efficient integrated power electronics, rf devices, and systems.

IV. CONCLUSIONS

In summary, voltage-impulse-induced nonvolatile ME tunable inductors are developed based on Metglas/(011) PMN-PT multiferroic composites by voltage-induced strain-mediated magnetic anisotropy. It exhibits high-inductance tunability up to 250% at 10 kHz and 120% at 1 MHz. This giant nonvolatile tunability is due to the large in-plane lattice-strain change from stable and reversible non-180° ferroelastic domain switching in PMN-PT single crystals. As non-180° ferroelastic domain switching is a universal phenomenon in ferroelectric materials, our study provides a pathway to achieve nonvolatile electrically tunable inductors for power-efficient integrated power electronics, rf devices, and systems.

ACKNOWLEDGMENTS

The work is supported by the Natural Science Foundation of China (Grants No. 51472199 and No. 11534015), the Natural Science Foundation of Shaanxi Province (Grant No. 2015JM5196), the National 111 Project of China (Grant No. B14040), the 973 program (Grant No. 2015CB057402), the China Postdoctoral Science Foundation (Grant No. 2016M590939), and the Fundamental Research Funds for the Central Universities. M. L. is supported by the China Recruitment Program of Global Youth Experts.

[1] D. S. Gardner, G. Schrom, F. Paillet, B. Jamieson, T. Karnik, and S. Borkar, Review of on-chip inductor structures with magnetic films, IEEE Trans. Magn. **45**, 4760 (2009).

[2] B. Axelrod, Y. Berkovich, and A. Ioinovici, Switched-capacitor/switched-inductor structures for getting transformerless hybrid dc-dc PWM converters, IEEE Trans. Circuits Syst. I Regul. Pap. **55**, 687 (2008).

[3] H. Su, X. L. Tang, H. W. Zhang, and N. X. Sun, Voltage-impulse-induced nonvolatile tunable magnetoelectric inductor based on multiferroic bilayer structure, Appl. Phys. Express **9**, 077301 (2016).

[4] G. X. Liu, X. X. Cui, and S. X. Dong, A tunable ring-type magnetoelectric inductor, J. Appl. Phys. **108**, 094106 (2010).

[5] H. Lin, J. Lou, Y. Gao, R. Hasegawa, M. Liu, B. Howe, J. Jones, G. Brown, and N. X. Sun, Voltage tunable magnetoelectric inductors with improved operational frequency and quality factor for power electronics, IEEE Trans. Magn. **51**, 4002705 (2015).

[6] J. Lou, D. Reed, M. Liu, and N. X. Sun, Electrostatically tunable magnetoelectric inductors with large inductance tunability, Appl. Phys. Lett. **94**, 112508 (2009).

[7] F. Khan, Y. Zhu, J. Lu, and J. Pal, MEMS-based tunable meander inductor, Electron. Lett. **51**, 1582 (2015).

[8] M. Mandal, S. P. Duttagupta, and V. R. Palkar, Fabrication and characterization of tunable multiferroic $Bi_{0.7}Dy_{0.3}FeO_3$ based on-chip micro-inductor, Microelectron. Eng. **106**, 38 (2013).

[9] M. Mandal, S. P. Duttagupta, and V. R. Palkar, Study of multiferroic $Bi_{0.7}Dy_{0.3}FeO_3$ based tunable ring inductor, J. Phys. D **46**, 325001 (2013).

[10] M. Rais-Zadch, P. A. Kohl, and F. Ayazi, MEMS switched tunable inductors, J. Microelectromech. Syst. **17**, 78 (2008).

[11] M. A. Y. Abdalla, K. Phang, and G. V. Eleftheriades, Printed and integrated CMOS positive/negative refractive-index phase shifters using tunable active inductors, IEEE Trans. Microwave Theory Tech. **55**, 1611 (2007).

[12] B. M. F. Rahman, R. Divan, D. Rosenmann, T. X. Wang, Y. J. Peng, and G. A. Wang, Application of sub-micrometer patterned permalloy thin film in tunable radio frequency inductors, J. Appl. Phys. **117**, 17C121 (2015).

[13] N. Ning, X. P. Li, J. Fan, W. C. Ng, Y. P. Xu, X. Qian, and H. L. Seet, A tunable magnetic inductor, IEEE Trans. Magn. **42**, 1585 (2006).

[14] M. Vroubel, Y. Zhuang, B. Rejaei, and J. N. Burghartz, Integrated tunable magnetic RF inductor, IEEE Electron Device Lett. **25**, 787 (2004).

[15] S. S. Bedair, J. S. Pulskamp, C. D. Meyer, R. G. Polcawich, and I. M. Kierzewski, Modeling, fabrication and testing of MEMS tunable inductors varied with piezoelectric actuators, J. Micromech. Microeng. **24**, 095017 (2014).

[16] S. S. Bedair, J. S. Pulskamp, C. D. Meyer, M. Mirabelli, R. G. Polcawich, and B. Morgan, High-performance micromachined inductors tunable by lead zirconate titanate actuators, IEEE Electron Device Lett. **33**, 1483 (2012).

[17] D. M. Fang, Q. A. Yuan, X. H. Li, and H. X. Zhang, Electrostatically driven tunable radio frequency inductor, Microsyst. Technol. **16**, 2119 (2010).

[18] J. I. Kim and D. Peroulis, Tunable MEMS spiral inductors with optimized RF performance and integrated large-displacement electrothermal actuators, IEEE Trans. Microwave Theory Tech. **57**, 2276 (2009).

[19] X. Fang, N. Zhang, and Z. L. Wang, Converse magnetoelectric effects on heterotype electrostrain-piezopermeability composites, Appl. Phys. Lett. **93**, 102503 (2008).

[20] M. Liu, O. Obi, Z. H. Cai, J. Lou, G. M. Yang, K. S. Ziemer, and N. X. Sun, Electrical tuning of magnetism in Fe_3O_4/PZN-PT multiferroic heterostructures derived by reactive magnetron sputtering, J. Appl. Phys. **107**, 073916 (2010).

[21] D. C. Lupascu and J. Rodel, Fatigue in bulk lead zirconate titanate actuator materials: A review, Adv. Eng. Mater. **7**, 882 (2005).

[22] J. M. Hu, L. Q. Chen, and C. W. Nan, Multiferroic heterostructures integrating ferroelectric and magnetic materials, Adv. Mater. **28**, 15 (2016).

[23] T. Wu, A. Bur, P. Zhao, K. P. Mohanchandra, K. Wong, K. L. Wang, C. S. Lynch, and G. P. Carman, Giant electric-field-induced reversible and permanent magnetization reorientation on magnetoelectric Ni/(011) $[Pb(Mg_{1/3}Nb_{2/3})O_3]_{(1-x)}$-$[PbTiO_3]_x$ heterostructure, Appl. Phys. Lett. **98**, 012504 (2011).

[24] M. Liu, B. M. Howe, L. Grazulis, K. Mahalingam, T. X. Nan, N. X. Sun, and G. J. Brown, Voltage-impulse-induced non-volatile ferroelastic switching of ferromagnetic resonance for reconfigurable magnetoelectric microwave devices, Adv. Mater. **25**, 4886 (2013).

[25] M. Liu *et al.*, Electrically controlled non-volatile switching of magnetism in multiferroic heterostructures via engineered ferroelastic domain states, NPG Asia Mater. **8**, e316 (2016).

[26] B. Noheda, D. E. Cox, G. Shirane, J. Gao, and Z. G. Ye, Phase diagram of the ferroelectric relaxor $(1-x)PbMg_{1/3}Nb_{2/3}O_3$-$xPbTiO_3$, Phys. Rev. B **66**, 054104 (2002).

[27] T. Wu, P. Zhao, M. Q. Bao, A. Bur, J. L. Hockel, K. Wong, K. P. Mohanchandra, C. S. Lynch, and G. P. Carman, Domain engineered switchable strain states in ferroelectric (011) $[Pb(Mg_{1/3}Nb_{2/3})O_3]_{(1-x)}$-$[PbTiO_3]_x$ (PMN-PT, x approximate to 0.32) single crystals, J. Appl. Phys. **109**, 124101 (2011).

[28] Metglas2601SA1, http://www.metglas.com/products/magnetic_materials/2605SA1.asp.

[29] Y. Shirahata, R. Shiina, D. L. Gonzalez, K. J. A. Franke, E. Wada, M. Itoh, N. A. Pertsev, S. van Dijken, and T. Taniyama, Electric-field switching of perpendicularly magnetized multilayers, NPG Asia Mater. **7**, e198 (2015).

[30] K. G. Webber, E. Aulbach, T. Key, M. Marsilius, T. Granzow, and J. Rodel, Temperature-dependent ferroelastic switching of soft lead zirconate titanate, Acta Mater. **57**, 4614 (2009).

[31] L. Jin, F. Li, and S. J. Zhang, Decoding the fingerprint of ferroelectric loops: Comprehension of the material properties and structures, J. Am. Ceram. Soc. **97**, 1 (2014).

[32] Y. Saito, H. Takao, T. Tani, T. Nonoyama, K. Takatori, T. Homma, T. Nagaya, and M. Nakamura, Lead-free piezoceramics, Nature (London) **432**, 84 (2004).